Fabrication and Testing of $l = 2$ Optical Vortex phase masks for Coronography

Elettra Mari,[1,*] Gabriele Anzolin,[2] Fabrizio Tamburini,[3] Mauro Prasciolu,[4] Gabriele Umbriaco,[3] Antonio Bianchini,[3] Cesare Barbieri,[3] and Filippo Romanato, [4,5,6]

[1]*CISAS "G.Colombo", University of Padua, Via Venezia 15 35131, Padova, Italy*
[2]*ICFO - Institut de Ciéncies Fotòniques, Mediterranean Technology Park, Av. del Canal Olìmpic 08860 Castelldefels (Barcelona), Spain*
[3]*Department of Astronomy, University of Padua, Vicolo dell'Osservatorio 3, 35122 Padova, Italy*
[4]*CNR-INFM TASC National Laboratory, S.S.14 Km 163.5, Area Science Park, 34012 Basovizza, Trieste, Italy*
[5]*Department of Physics, University of Padua, Via F. Marzolo 8, 35131 Padova, Italy*
[6]*LaNN, Laboratory for Nanofabrication of Nanodevices, Veneto Nanotech, Via San Crispino 106, 35129 Padova, Italy*
**elettra.mari@unipd.it*

Abstract: In this paper we present the fabrication process and tests of two different types of $l = 2$ spiral phase plates (SPPs), designed for an Optical Vortex Coronagraph (OVC) in the visible wavelength regime. Each phase mask is realized dividing the spirals area in sectors respectively of 8 and 512 of levels using lithographic nanofabrication approach. The SPPs produces different optical vortices (OVs) with topological charge l that depends on the number of steps and on the wavelength. We found that the residual light in the central dark region of the OV tends to zero as the number of steps increases.

OCIS codes: (050.4865) Optical vortices; (050.1970) Diffractive optics; (350.1260) Astronomical optics; (110.6895) Three-dimensional lithography

References and links

1. L. Allen, M. W. Beijersbergen, R. J. C. Spreeuw, and J. P. Woerdman, "Orbital angular momentum of light and the transformation of Laguerre-Gaussian laser modes," Phys. Rev. A **45**(11), 8185–8189 (1992).
2. G. Anzolin, F. Tamburini, A. Bianchini, and C. Barbieri, "Method to measure off-axis displacements based on the analysis of the intensity distribution of a vortex beam," Phys. Rev. A **79**(3), 033845 (2009).
3. A. Vaziri, G. Weihs, and A. Zeilinger, "Superpositions of the orbital angular momentum for applications in quantum experiments," J. Opt. B Quantum Semiclassical Opt. **4**(2), 367 (2002).
4. G. Anzolin, F. Tamburini, A. Bianchini, G. Umbriaco, and C. Barbieri, "Optical vortices with starlight," Astron. Astrophys. **488**(3), 1159–1165 (2008).
5. M. Harwit, "Photon Orbital Angular Momentum in Astrophysics," Astrophys. J. **597**(2), 1266–1270 (2003).
6. B. Thidé, H. Then, J. Sjöholm, K. Palmer, J. Bergman, T. D. Carozzi, Y. N. Istomin, N. H. Ibragimov, and R. Khamitova, "Utilization of photon orbital angular momentum in the low-frequency radio domain," Phys. Rev. Lett. **99**(8), 087701 (2007).
7. F. Tamburini, G. Anzolin, G. Umbriaco, A. Bianchini, and C. Barbieri, "Overcoming the Rayleigh Criterion Limit with Optical Vortices," Phys. Rev. Lett. **97**(16), 163903 (2006).
8. J. H. Lee, G. Foo, E. G. Johnson, and G. A. Swartzlander, Jr., "Experimental verification of an optical vortex coronagraph," Phys. Rev. Lett. **97**(5), 053901 (2006).
9. G. Foo, D. M. Palacios, and G. A. Swartzlander, Jr., "Optical vortex coronagraph," Opt. Lett. **30**(24), 3308–3310 (2005).
10. D. Mawet, P. Riaud, O. Absil, and J. Surdej, "Annular Groove Phase Mask Coronagraph," Astrophys. J. **633**(2), 1191–1200 (2005).
11. E. B. Kley, "Continuous profile writing by electron and optical lithography," Microelectron. Eng. **34**(3-4), 261–298 (1997).
12. D. Ganic, X. Gan, M. Gu, M. Hain, S. Somalingam, S. Stankovic, and T. Tschudi, "Generation of doughnut laser beams by use of a liquid-crystal cell with a conversion efficiency near 100%," Opt. Lett. **27**(15), 1351–1353 (2002).
13. Q. Wang, X. W. Sun, P. Shum, and X. J. Yin, "Dynamic switching of optical vortices with dynamic gamma-correction liquid crystal spiral phase plate," Opt. Express **13**(25), 10285–10291 (2005).
14. M. Prasciolu, F. Tamburini, G. Anzolin, E. Mari, M. Melli, A. Carpentiero, C. Barbieri, and F. Romanato, "Fabrication of a three-dimensional optical vortices phase mask for astronomy by means of electron-beam lithography," Microelectron. Eng. **86**(4-6), 1103–1106 (2009).

#120587 - $15.00 USD Received 30 Nov 2009; revised 18 Dec 2009; accepted 19 Dec 2009; published 21 Jan 2010

15. S. S. R. Oemrawsingh, J. A. W. van Houwelingen, E. R. Eliel, J. P. Woerdman, E. J. K. Verstegen, J. G. Kloosterboer, and G. W. 't Hooft, "Production and characterization of spiral phase plates for optical wavelengths," Appl. Opt. **43**(3), 688–694 (2004).
16. C.-S. Guo, D.-M. Xue, Y.-J. Han, and J. Ding, "Optimal phase steps of multi-level spiral phase plates," Opt. Commun. **268**(2), 235–239 (2006).
17. G. A. Swartzlander, Jr., "Achromatic optical vortex lens," Opt. Lett. **31**(13), 2042–2044 (2006).

1. Introduction

Optical vortices (OVs) are topological defects due to phase singularities in light beams carrying orbital angular momentum (OAM). In cylindrical coordinates, in the plane orthogonal to the beam propagation direction, z, the Electromagnetic field can be described in terms of a superposition of L-G modes, whose amplitude z is given by

$$u_{lp}(r,\theta) \propto \left(\frac{r\sqrt{2}}{w_0}\right)^{|l|} L_p^{|l|}\left(\frac{2r^2}{w_0^2}\right)\exp\left(-\frac{r^2}{w_0^2}\right)\exp(-il\theta) \qquad (1)$$

where l is the azimuthal index indicating the number of twists of the helical wavefront within a wavelength, w_0 is the beam waist, $L_p^{|l|}$ is the correspondent Laguerre polynomial, p the number of radial nodes present in the LG mode and l is the so-called "topological charge". The phase varies linearly with the azimuthal angle, θ, as expressed by the term $\exp(-il\theta)$. At the single photon regime, each photon of the beam carries an OAM equal to $l\hbar$ [1]. The most commonly optical devices used to generate OVs are the phase modifying devices (PMD) such as computer-generated fork holograms (FH) and spiral phase plates (SPP). The SPP is a helicoidal transmission optical element that looks like a spiral staircase with a certain number of steps that progressively build the total phase gap h_s after a complete rotation of the azimuthal angle θ. When the number of steps N is finite, we have a Multi-level Spiral Phase Plate (MLSPP) and each step introduces a constant phase variation; when N tends to infinity, we have a continuous phase mask (CSPP) and the phase of the light is modulated smoothly and continuously (Fig. 1).

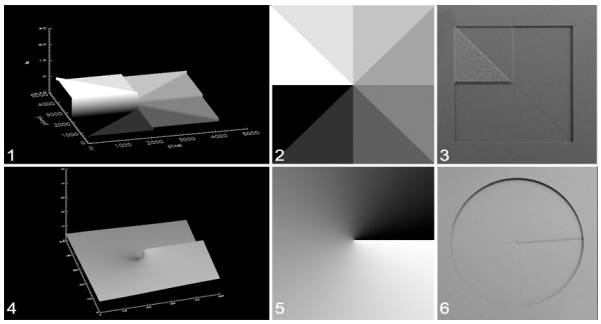

Fig. 1. Top panels (1, 2 and 3) N = 8 MLSPP and lower panels (4, 5 and 6) MLSPP with 512 steps. On the left: simulated three-dimensional images (1 and 4), the corresponding phase delay introduced by each single step (2), and that varies continuously as a function of the azimuthal angle (5). On the right are shown SEM images of the actual MLSPPs carved in the PMMA (3 and 6).

A monochromatic Gaussian light beam, crossing on axis the PMD, is transformed into a superposition of Laguerre-Gaussian (LG) or Kummer modes [2], whose intensity profiles assume a doughnut-like shape, characterized by a circular symmetry with a central dark zone. When the beam intersects the PMD away from its center, the intensity profile of the OV is described by a superposition of different L-G modes, that looses the axial symmetry and the intensity distribution tends to concentrate towards a Gaussian beam [3]. In this paper we analyze only the properties of SPPs, because they produce OVs along the same optical axis and, for this reason, can be more appropriately used at the telescope. A non-monochromatic

#120587 - $15.00 USD Received 30 Nov 2009; revised 18 Dec 2009; accepted 19 Dec 2009; published 21 Jan 2010

beam crossing a SPP, produces a series of concentric, on-axis OVs with different topological charges for each different wavelength. The FH, instead, produces infinite superposed and laterally dispersed OVs with equal l along the spectrum of a star, with a resulting non-null intensity in the central region and thus does not meet our present needs. Recently, OVs became a widely discussed topic in both optical and radio astronomy [4–6]. Tamburini et al. [7] demonstrated that imposing OAM to the light collected by a telescope the resolving power can been improved up to an order of magnitude below the Rayleigh criterion limit in white light and even up to 50 times if one uses monochromatic and coherent sources. OVs have also been proposed for the direct detection of extrasolar planets. The diffraction pattern of the host star, when on-axis, is transformed by a PMD into an even-topologically charged OV collimated by the lens L3, and its doughnut-shaped light distribution is blocked by an annular Lyot stop (LS) [8–10]. Only the light coming from the off-axis source, will skip the Lyot stop to be detected. The use of an even-valued topological charge l is mandatory to perform high contrast coronagraphy. In fact, only in this case, the central region of the OV generated by the main star is completely dark, due to destructive interference occurring inside the vortex [10]. In this paper we illustrate the fabrication process and the optical tests of two different types of monochromatic, $l = 2$, SPPs that differ from each other by the number of steps used to build the total phase gap. Each mask is designed to work in the visible light ($\lambda_0 = 550$nm).

2. Fabrication process

The SPP was fabricated by means of Electron Beam Lithography (EBL). EBL is a nanofabrication technique that permits the fabrication of continuous surface profiles in three-dimensional (3D) shapes, offering high flexibility in the elements design with good optical quality and satisfying the requirements of micro-optics [11]. The core of EBL process is the interaction between highly energetic electron beams and an electron-sensitive polymer material, called resist. The electron beam, entering the resist film, loses energy via elastic and inelastic collisions, namely electron scattering. The 3D profiles are obtained by changing locally the electron dosage, inducing changes in the dissolution rate of polymer film. After the development process, zones of polymer having different thicknesses are obtained. For our experiments we have patterned a series of MLSPPs with 8 or 512 levels. The side of the squared MLSPP and the diameters of the other two circular masks are 1 mm wide. The 3D-spiral phase mask profiles were directly written on a 2.7 mm-thick polymethyl-methacrylate (PMMA) slide clinical grade free from Ultra-Violet absorber. The 2.7mm PMMA slide used for the fabrication of the masks has high electrical resistivity, of the order the 10^{15} Ohm·cm, that creates a charging effect highly affecting the EBL writing. On the top of the PMMA slide was deposed by evaporation a 50 nm-thick aluminum film to avoid electrostatic charging. The thin layer was grounded with the EBL chuck, thus discarding the slide during the EBL writing. The metal layer can easily be removed in a 10:1 HF (10 H_2O: 1 HF 48%) solution bath before the development step. The 10:1 HF solution etching rate on PMMA is negligible. Electron-beam exposure was carried out at 30 kV with a beam probe currents of 100pA. The development process was performed in GG developer bath, a mixture of diethylene-glycol-monobutyl ether, morpholine, ethanolamine and deionized water, at 25°C for 30 minutes and rinsed in de-ionized water. We have not used liquid crystal SPPs [12,13] because they have both a smaller spatial resolution and a smaller number of steps than those provided by EBL. So, at the moment, LC-SPPs do not seem to match OVC requirements. More details can be found in Ref [14].

3. Numerical simulations

The topological charge l of the OVs produced by the SPP depends on the jump h_s, the wavelength λ_0 at which the maximum fainting of the on-axis source is obtained, and on Δn, namely the difference between the refractive index of the SPP and that of the surrounding medium

$$l = \Delta n \cdot h_s / \lambda_0 \qquad (2)$$

#120587 - $15.00 USD Received 30 Nov 2009; revised 18 Dec 2009; accepted 19 Dec 2009; published 21 Jan 2010

For a CSPP see Ref [15]. The theoretical behavior described by Eq. (2) is not fully matched by MLSPPs. In fact, the topological charge of the OVs depends also on the number of the steps used to build the total phase gap. Because of the stepped structure the central dark zone of the OV is partially filled by the light of the additional L-G terms. In other words, the steps interfere with the fundamental OAM mode of Eq. (2) modifying its intensity distribution [16]. This implies that, for given h_s and Δn, the maximum fainting inside the OV is obtained at a wavelength different than λ_0. We developed a numerical code in IDL to reproduce the behavior of a CSPP and MLSPPs with different number of steps, assuming $l = 2$ in Eq. (2). When the Airy diffraction pattern, like that produced by a star imaged by an ideal telescope without obstructions, intersects the MLSPP in its optical singularity, the IDL routine calculates the output image point by point using the Fourier imaging technique. Our SPPs and the Airy patterns of the simulated stellar sources were encoded in 4096×4096 matrices. The intensities of the stellar sources were normalized to unity. The fainting produced by the phase mask is defined as the ratio between the light passing through the SPP and the Lyot stop, and the light that should pass through the same circular area when the phase mask is removed. The values of the maximum fainting obtained for the CSPP (indicated by "∞") and for MLSPPs having 8, 16, 32, 64, 128 and 512 steps, are reported in Tab. (1) together with the wavelength at which the fainting is minimum

Table 1. Maximum fainting of light passing through the MLSPP and the Lyot stop and the corresponding maximum efficiency wavelength as a function of the wavelength.

N step	8	16	32	64	128	512	∞
Fainting	$2.39 \cdot 10^{-2}$	$7.14 \cdot 10^{-3}$	$1.94 \cdot 10^{-3}$	$4.98 \cdot 10^{-4}$	$1.27 \cdot 10^{-4}$	$1.17 \cdot 10^{-5}$	$2.68 \cdot 10^{-6}$
λ_{min}	624	585	567	558	554	550	550

These results show a clear dependence between the number of steps and the wavelength at which the maximum fainting of light at the centre of the OV is obtained. Of course, the value of the fainting reached by a CSPP should be zero, but the result is limited by the numerical errors. Figure 2 shows the relationship between the number of steps of the MLSPP and the wavelength (λ_{min}^{N}) **at which the maximum fainting is obtained, with an asymptotic beh**avior at λ_0 for a CSPP.

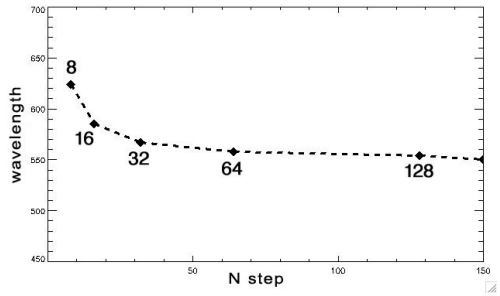

Fig. 2. Maximum efficiency λ for different MLSPPs. vs. number of steps.

From our numerical results we obtain an approximated relationship linking the wavelength at which the maximum fainting of light is found for our CSPPs (λ_{min}^{∞}) and for the *N*-step MLSPP,

$$\lambda_{min}^{N} = \lambda_{min}^{\infty} + \lambda_{min}^{\infty} / N \qquad (3)$$

From Eq. (2) and Eq. (3) one obtains the relationship between *l* and *N* at a given wavelength when the fainting is maximum,

#120587 - $15.00 USD Received 30 Nov 2009; revised 18 Dec 2009; accepted 19 Dec 2009; published 21 Jan 2010

$$l = \frac{\Delta n \cdot h_s}{\lambda}\left(\frac{N+1}{N}\right) \tag{4}$$

Figure 3 shows the fainting for each of the MLSPPs (8, 16, 32 steps) and for the CSPP with respect to the wavelength. The intensity scale has been normalized to that of a beam without any loss.

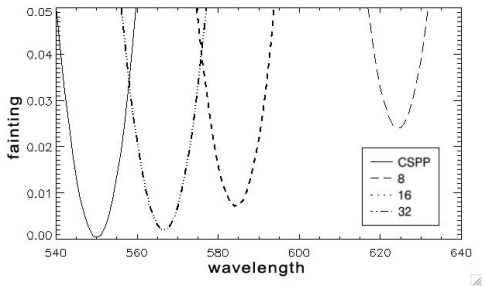

Fig. 3. Fainting efficiency of the MLSPPs and of the ideal CSPP vs. the wavelength.

The dependence of the attenuation from the wavelength and the number of steps causes problems of chromaticity and contrast for the OVC; the best attenuation can be obtained with a CSPP within a narrow-band around the maximum efficiency wavelength. We estimate that a shift of ± 10 nm corresponds to a loss of contrast of about two orders of magnitude. This problem can be partially solved with the use of an achromatic SPP [17].

4. Laboratory tests

Here we report the laboratory tests of two different MLSPPs, for optical vortex coronagraphy, with $N = 8$, and $N = 512$, having the same central step of 2.2 μm. At the telescope it is not always possible to work in monochromatic regime because of the faintness of the sources. For this reason, we are interested to study the behavior of the phase mask also at wavelengths different than λ_0, for which the mask was designed. To this end, we tested the MLSPPs using a high quality He-Ne CW laser beam with $\lambda = 632.8$ nm and compared the results with the numerical simulations. The optical setup reproduces the focal ratio *f /16* of the Cassegrain configuration of the T122 Asiago Telescope (Fig. 4), which reasonably approximates the paraxial regime of the beam.

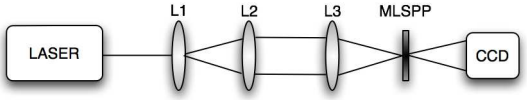

Fig. 4. Schematic diagram of the setup used in laboratory. L1 and L2 are lenses that form a beam expander, L3 focuses light on the center of the SPP.

All images were recorded with a 1024 x 768 24-Bit Color CCD camera. Figure 5 shows the agreement between experimental and numerical results obtained a MLSPP with $N = 8$, while in the right those with $N = 512$.

#120587 - $15.00 USD Received 30 Nov 2009; revised 18 Dec 2009; accepted 19 Dec 2009; published 21 Jan 2010

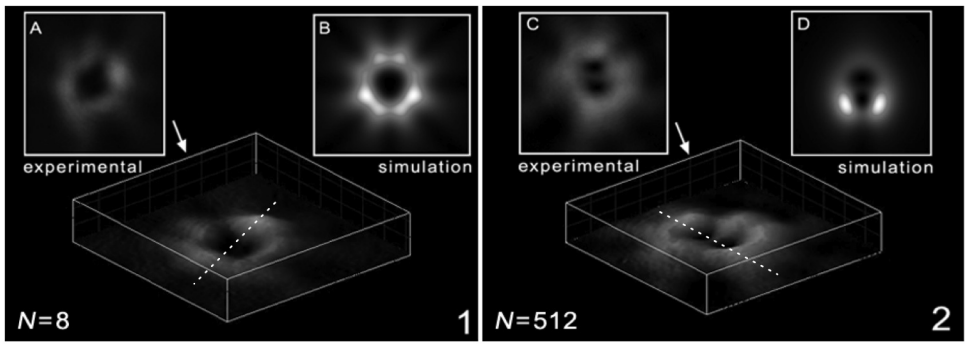

Fig. 5. Experimental (A and C) and simulated (B and D) optical vortices obtained using SPP with $N = 8$ (panel 1) and $N = 512$ (panel 2). Experimental results are also shown in 3D, where dotted lines indicate the locations of the profiles reported in Fig. 6.

Figure 6 shows the intensity profiles of the simulated (continuous line) and experimental (dash-dotted) OVs plotted with normalized intensities to put in evidence the existing similarities.

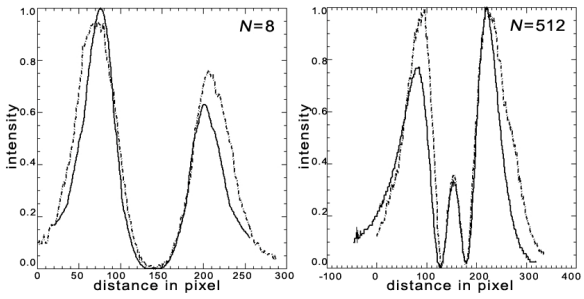

Fig. 6. The profiles of the OVs shown in Fig. 5.

The different patterns observed in the two panels are due to the different topological charges of the OVs as predicted by Eq. (4). In fact, for $N = 8$ one expects to achieve the maximum fainting at $\lambda_{min} = 624$ nm, that is quite close to that of the laser. For this reason, the OV profiles of left panel present the expected central dark region. For $N = 512$, instead, the prediction is $\lambda_{min} = 550$ nm, so the light of our laser partially fills the central OV region with fractional OAM values, as shown in the right panel of Fig. 6. The main differences observed between the numerical simulations and the corresponding experimental results are partially due to possible imperfections in the optical quality of the mask and/or to small misalignments in the optical setup affecting the symmetric shape of the OV.

5. Conclusions

In this paper we have analyzed the properties of MLSPPs at different wavelengths for future application in OVC. We have shown both numerically and experimentally that the topological charge of the OVs produced by MLSPPs depend on the number of steps N to build phase gap, even if the materials and the height of the total phase jump are the same. The number of steps N is crucial for the efficiency of the OVC.

Acknowledgements

This work has been partially supported by the University of Padova, by the Ministry of University and Research and by the CARIPARO Foundation inside the 2006 Program of Excellence.

#120587 - $15.00 USD Received 30 Nov 2009; revised 18 Dec 2009; accepted 19 Dec 2009; published 21 Jan 2010